

FlexCausal: Flexible Causal Disentanglement via Structural Flow Priors and Manifold-Aware Interventions

Yutao Jin¹ Yuang Tao¹ Junyong Zhai¹

Abstract

Causal Disentangled Representation Learning (CDRL) aims to learn and disentangle low dimensional representations and their underlying causal structure from observations. However, existing disentanglement methods rely on a standard mean-field approximation with a diagonal posterior covariance, which decorrelates all latent dimensions. Additionally, these methods often assume isotropic Gaussian priors for exogenous noise, failing to capture the complex, non-Gaussian statistical properties prevalent in real-world causal factors. Therefore, we propose FlexCausal, a novel CDRL framework based on a block-diagonal covariance VAE. FlexCausal utilizes a Factorized Flow-based Prior to realistically model the complex densities of exogenous noise, effectively decoupling the learning of causal mechanisms from distributional statistics. By integrating supervised alignment objectives with counterfactual consistency constraints, our framework ensures a precise structural correspondence between the learned latent subspaces and the ground-truth causal relations. Finally, we introduce a manifold-aware relative intervention strategy to ensure high-fidelity generation. Experimental results on both synthetic and real-world datasets demonstrate that FlexCausal significantly outperforms other methods.

1. Introduction

Causality (Pearl, 2009) has significantly advanced modern artificial intelligence, enabling agents not only to observe patterns, but also to comprehend the underlying mechanisms governing the world. Despite unprecedented success in fitting statistical correlations, contemporary deep learning often encounters challenges at higher levels of the "causal ladder", specifically in intervention analysis and counterfactual reasoning. Unlike traditional Disentangled Representa-

¹Southeast University, Jiangsu, China. Correspondence to: Yutao Jin <yutao0212@seu.edu.cn>, Yuang Tao <yuangtao@seu.edu.cn>, Junyong Zhai <jyzhai@seu.edu.cn>.

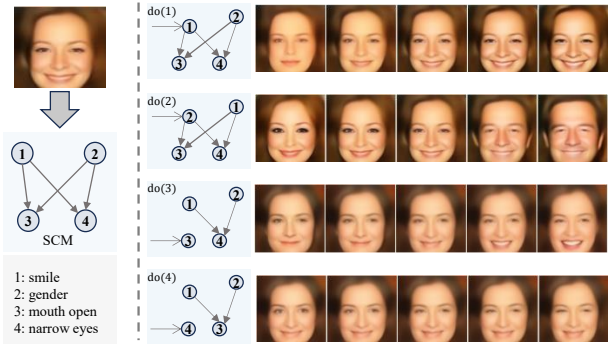


Figure 1. CRDL aims to disentangle latent causal factors from observation and enable controllable causal generation. Our FlexCausal effectively disentangles causal representations. Interventions on parent nodes will influence their child nodes, while interventions on child nodes leave the parent nodes invariant.

tion Learning (DRL) methods, which focus on the statistical independence of latent factors, Causal Disentangled Representation Learning (CDRL) (Schölkopf et al., 2021; Yang et al., 2021) shifts the focus toward uncovering the structural causal mechanisms governing high-dimensional semantic concepts. As demonstrated in Figure 1, by disentangling and controlling these causal representations, deep learning models can facilitate various real-world tasks, ranging from controllable factual synthesis to counterfactual generation. To this end, recent advances have integrated causal semantics into various generative frameworks to enable counterfactual image editing, including VAEs (Yang et al., 2021; Komanduri et al., 2022), GANs (Kocaoglu et al., 2018), and Diffusion models (Komanduri et al., 2024b; Huang et al., 2025).

Despite these advances, existing CDRL frameworks often fail when applied to complex real-world systems, primarily because they fail to mitigate two fundamental limitations. First, they typically rely on the restrictive Gaussian assumption, which fails to capture the complex, non-Gaussian distributions found in real-world data, thereby limiting identifiability. Second, there is a mismatch between the modeled latent structure and the true causal geometry. Standard approaches often ignore the intra-concept block-wise correlations and rely on naive hard interventions that neglect the data manifold. This structural misalignment inevitably results in unrealistic counterfactuals that violate the consis-

tency needed for reliable generation.

Therefore, we propose FlexCausal, a novel CDRL framework aimed at combining structural causal modeling with flexible density estimation. FlexCausal achieves the disentanglement of high-dimensional causal representations by learning independent Normalizing Flows for each concept's exogenous priors, while enforcing strict causal consistency among latent variables during training. It is crucial that FlexCausal facilitates manifold-aware interventions, allowing for counterfactual generation that strictly adheres to the topological structure of each latent concept. By relaxing rigid distributional assumptions and respecting the geometry of data, FlexCausal effectively fosters causal disentanglement and mitigates distributional mismatch in complex real-world scenarios.

Specifically, we introduce a Flow-based Exogenous Prior framework that employs invertible normalizing flows to explicitly model the complex distributions of exogenous variables, effectively relaxing the rigid constraints inherent in traditional causal VAEs like CausalVAE. Furthermore, we propose a Manifold-Aware Directional Intervention mechanism coupled with a Counterfactual Consistency Loss. Different from traditional hard interventions that rely on arbitrary scalar assignments, this mechanism learns semantic directions within a designed Block-Diagonal latent space and performs soft interventions along the natural data manifold.

Overall, our main contributions are summarized as follows:

- We propose a novel CDRL framework named FlexCausal that synergizes SCMs with deep generative learning via an additive Flow-based prior. By enforcing a strict Block-Diagonal constraint on the posterior distributions and explicitly learning complex exogenous priors, our approach successfully disentangles high-dimensional causal concepts.
- We introduce an additive Flow-based Exogenous Prior that imposes a strict Block-Diagonal constraint on the latent covariance, while simultaneously enforcing a counterfactual consistency constraint during training. This design fundamentally overcomes the theoretical limitations of conventional methods by relaxing rigid Gaussian assumptions and intra-dimensional independence.
- We propose a novel intervention strategy designed to perceive the direction of the original data manifold. Unlike hard interventions that often yield off-manifold artifacts, our method performs relative interventions along learned semantic directions. This ensures that counterfactual generation maintains high fidelity while strictly adhering to the underlying geometric structure of the data.

- We construct Filter, a new synthetic benchmark where latent concepts are sampled from different complex distributions to simulate real-world environmental complexity. Experimental results demonstrate that our FlexCausal outperforms other methods on both synthetic datasets and standard real-world datasets.

2. Related Works

2.1. Disentangled Representation Learning and Causal Representation Learning

With the development of deep learning, Disentangled Representation Learning (DRL) has emerged as a method capable of extracting independent and interpretable low-dimensional representations from high-dimensional (Bhowal et al., 2024). The core goal of DRL is to map observations into a latent space where distinct semantic factors are encoded into independent dimensions (Bengio et al., 2013). Previous works such as β -VAE (Higgins et al., 2017) and FactorVAE (Duan et al., 2022) achieve this by enforcing statistical independence of latent variables, typically employing a KL divergence penalty mechanism between the posterior distribution and a standard Gaussian prior. However, the strict independence assumption in DRL faces significant theoretical and practical challenges. Theoretically, (Locatello et al., 2019) proved that unsupervised disentanglement is impossible without inductive biases. Practically, statistical independence among semantic factors rarely exists in real-world scenarios. To address these limitations, Causal Representation Learning (CRL) (Schölkopf et al., 2021) focuses on structural causal disentanglement. By integrating SCMs into the representation learning process, CRL aims to uncover causal relationships among latent variables, thereby enabling the recovery of causally related concepts and counterfactual reasoning. Nevertheless, most existing CRL frameworks (Buchholz et al., 2023; Lippe et al., 2023) are still built upon the restrictive assumption of standard Gaussian priors for exogenous variables. Recent frontier works (Zhang et al., 2024; Kori et al., 2025) have begun to explore CRL approaches based on mixture priors to better learn the complex, multi-modal causal representation in real-world scenarios.

2.2. Causal Disentangled Representation Learning

Different from DRL's strict assumption of statistical independence, Causal Disentangled Representation Learning (CDRL) instantiates the theoretical principles of CRL by explicitly integrating SCMs into deep generative frameworks. This integration facilitates both robust causal representation learning and controllable causal generation. CausalVAE (Yang et al., 2021), introduces a specialized Causal Layer that transforms independent exogenous noise into causally endogenous variables via linear structural equa-

tions, effectively propagating causal effects during inference. DEAR (Shen et al., 2022) uses a GAN-based architecture combined with SCM priors to enable supervised learning of causal structures. Similarly, SCM-VAE (Komanduri et al., 2022) utilizes additive noise models alongside a fixed SCM to enhance both identifiability and interpretability. ICM-VAE (Komanduri et al., 2024a) employs flow-based diffeomorphic mappings to model nonlinear causal mechanisms under the Independent Causal Mechanisms (ICM) principle, achieving theoretically identifiable causal disentanglement. To Address the issue of confounders, CFI-VAE (Li et al., 2024) learns unbiased causal representations by eliminating data bias and C-Disentanglement (Liu et al., 2023) relaxes the traditional assumption of confounder-free data by explicitly incorporating the inductive bias of confounders, thereby improving the performance of disentanglement. Building upon the causal insights of CFI-VAE, CIDiffuser (Huang et al., 2025) incorporates Diffusion models to generate high quality counterfactual images.

2.3. Deep Generative Model and Counterfactual Editing

With the learned causal representation, Deep Generative Models (Goodfellow et al., 2020; Ho et al., 2020; Song et al., 2021) can be employed to generate both factual observations and counterfactual alternatives. (De Sousa Ribeiro et al., 2023) leverage Hierarchical VAEs to perform a strict Abduction-Action-Prediction procedure, achieving high-fidelity counterfactual generation with hard intervention. (Pan & Bareinboim, 2024; 2025) derive theoretical probability bounds within the Augmented SCM (ASCM) framework to establish Counterfactual Consistency, utilizing it primarily as a theoretical metric to verify if distributions fall within identifiable bounds. Distinguishing our work from these methods, FlexCausal reformulates counterfactual consistency from a theoretical constraint into a trainable loss function. By explicitly imposing structural penalties on latent vectors during training, we directly embed causal dynamics into the representation learning process.

Furthermore, addressing the limitations of hard intervention in previous studies (Shen et al., 2020; Fan et al., 2025), we propose a Manifold-Aware Directional Intervention strategy. This ensures that the generated counterfactuals traverse along the high-density geodesic of the learned manifold rather than being projected into invalid regions, thereby preserving the realism of the original data.

3. Primaries

We formulate causal representation learning within a VAE framework that maps the high-dimensional data points $x \in \mathcal{X} \subseteq \mathbb{R}^n$ and associated labels $u \in \mathcal{U} \subseteq \mathbb{R}^m$ to the latent variable $z \in \mathcal{Z} \subseteq \mathbb{R}^d$ ($d \ll n$). The model is defined by a conditional probabilistic encoder $q_\phi(z|x)$ that infers latent

causal factors given both the image and the label, and a generator $p_\theta(x|z)$ that reconstructs the observations.

Assumption 3.1 (Causal Factorize). The latent vector z partitions into disjoint causal vector blocks, denoted as $z = [z_1^\top, \dots, z_K^\top]^\top$. Each sub-vector $z_k \in \mathbb{R}^{d_k}$ ($\sum_{k=1}^K d_k = d$) functions as a coherent semantic unit, representing a high-dimensional node in the underlying causal graph.

Definition 3.2. A Structural Causal Model (SCM) is a tuple $(\mathbf{Z}, \mathbf{N}, \mathbf{F}, P_{\mathbf{N}})$, where:

- (1) $\mathbf{Z} = \{z_1, \dots, z_K\}$ is a set of endogenous latent variables.
- (2) $\mathbf{N} = \{n_1, \dots, n_K\}$ is a set of exogenous noise variables.
- (3) $\mathbf{F} = \{f_1, \dots, f_K\}$ is a set of deterministic structural functions, where $z_k := f_k(\text{PA}(z_k), n_k)$ and $\text{PA}(z_k) \subseteq \mathbf{Z} \setminus \{z_k\}$ denotes the causal parents of z_k .
- (4) $P_{\mathbf{N}}$ is a product distribution over the exogenous noise.

The causal structure is represented by a Directed Acyclic Graph (DAG) \mathcal{G} , where a directed edge $z_j \rightarrow z_k$ exists if $z_j \in \text{PA}(z_k)$.

Assumption 3.3 (Latent Causal Sufficiency). A system is causally sufficient, meaning there are no unobserved latent confounders influencing multiple variables in \mathcal{Z} . Consequently, the exogenous noise variables are mutually independent:

$$p(n) = \prod_{k=1}^K p(n_k). \quad (1)$$

This implies that the root nodes of \mathcal{G} are mutually independent, and for any node z_k , its dependence on the rest of the graph is fully mediated by its causal parents $\text{PA}(z_k)$.

Definition 3.4. An Additive Noise Model (ANM) (Hoyer et al., 2008) is defined as a structural causal system where each latent variable z_k is generated as a deterministic function of its causal parents $\text{PA}(z_k)$ superimposed with an independent additive noise term n_k :

$$z_k := f_k(\text{PA}(z_k)) + n_k, \quad k = 1, \dots, K \quad (2)$$

where $f_k(\cdot)$ denotes the nonlinear causal mechanism governed by the causal graph \mathcal{G} . In our implementation, the parent sets $\text{PA}(z_k)$ and the dependency structure of f_k are explicitly specified by a fixed prior adjacency matrix A .

Assumption 3.5 (Non-Gaussianity). To guarantee causal identifiability beyond the Markov equivalence class (Hoyer et al., 2008), we assume the distributions of the exogenous noise $p(n_k)$ are non-Gaussian (e.g., Laplace, Bimodal). This assumption justifies our use of Flow-based priors to capture complex distributional geometries.

Proposition 3.6. Let \mathcal{G} be a Directed Acyclic Graph (DAG) representing the causal structure. Under Definition 3.4, the

mapping $\mathcal{T} : \mathcal{Z} \rightarrow \mathcal{N}$ defined by $n_k = z_k - f_k(\text{PA}(z_k))$ is a volume-preserving bijective transformation. Specifically, the absolute determinant of its Jacobian matrix is unity:

$$\left| \det \frac{\partial n_k}{\partial z_k} \right| = 1. \quad (3)$$

This property implies that the log-likelihood in the causal latent space equates to the log-likelihood in the exogenous noise space, i.e., $\log p(z_k) = \log p(n_k)$.

4. Methodology

Figure 2 demonstrates the overall architecture of the proposed FlexCausal. Built upon a Block-Diagonal Variational Autoencoder (VAE) backbone, our model encodes observations into a disentangled latent space and captures nonlinear causal relationships among concepts using ANMs. We first derive the exogenous noise residuals n_k from the latent variables z_k using Equation 2 and then model their densities with invertible Normalizing Flows. Furthermore, we introduce an intervention-based Counterfactual Consistency Constraint. This mechanism penalizes violations of structural equations under causal intervention, thereby facilitating robust causal disentanglement and ensuring the reliability of counterfactual image generation.

4.1. Structure-Aware Representation Learning via Block-Diagonal VAE

Consistent with the ANM framework outlined in Definition 3.4, the observational data x is generated by a causal latent vector z . The underlying causal topology is pre-defined and encoded by a fixed binary adjacency matrix $A \in \{0, 1\}^{K \times K}$, and $A_{jk} = 1$ indicates the existence of a directed causal edge $z_j \rightarrow z_k$. Under this topological constraint, each variable z_k is structurally determined by its causal parents:

$$z_k = f_k(z_j \mid A_{jk} = 1) + n_k, \quad (4)$$

where $z_k \in \mathbb{R}^{d_k}$ represents a distinct vector-valued semantic concept, $f_k(\cdot)$ is a learnable nonlinear structural function, and n_k denotes the independent exogenous noise.

Standard VAEs, which are utilized in CausalVAE and SCM-VAE, typically employ a mean-field approximation. This formulation assumes a diagonal posterior covariance, effectively forcing all latent dimensions to be statistically independent. While this strategy facilitates the disentanglement of distinct concepts, it is detrimental to vector-valued concepts. Crucially, the dimensions within a single concept z_k are inherently coupled. Severing these intra-concept correlations compromises the semantic integrity and geometric structure of the causal variables.

To prevent the destruction of intra-concept correlations, we utilize a Block-Diagonal Variational Encoder E_ϕ . Our method not only disentangles distinct semantic concepts but also maintains the necessary dependencies within each concept block. We formulate the variational posterior as follow:

$$q_\phi(z|x) = \mathcal{N}(\mu_\phi(x), \Sigma_\phi(x)). \quad (5)$$

To achieve the causal factorization postulated in Assumption 3.1, the covariance matrix $\Sigma_\phi(x)$ is constrained to be block-diagonal. Specifically, we require zero correlations between distinct causal concepts z_k, z_j ($k \neq j$) while maintaining dense intra-concept dependencies. We construct $\Sigma_\phi(x)$ as the direct sum of concept-specific covariance blocks:

$$\Sigma_\phi(x) = \text{blkdiag}(\Sigma_1(x), \dots, \Sigma_k(x)). \quad (6)$$

To ensure positive definiteness and numerical stability, we parameterize each block Σ_k via its local Cholesky factor L_k . The global Cholesky matrix L is composed of these sub-blocks:

$$L = \text{blkdiag}(L_1, \dots, L_K), \quad (7)$$

where $L_k = \text{tril}(V_k)$, $V_k \in \mathbb{R}^{d_k \times d_k}$ denotes the raw output sub-matrix from the encoder corresponding to the k -th concept, and $\text{tril}(\cdot)$ enforces the lower-triangular constraint. The diagonal elements of each L_k are rectified via softplus. Consequently, the full covariance is given by $\Sigma_k = L_k L_k^\top$. The latent variables are then sampled via the reparameterization trick. Due to the block-diagonal structure, this can be performed independently for each concept:

$$z_k = \mu_k + L_k \epsilon_k, \quad \epsilon_k \sim \mathcal{N}(0, I) \quad (8)$$

Or in global vector form: $z = \mu + L\epsilon$.

4.2. Flow-based Exogenous Prior

Previous CDRL methods typically use a standard isotropic Gaussian prior as exogenous variables, i.e. $p(n) = \mathcal{N}(\mathbf{0}, I)$. Although mathematically convenient, this assumption is overly restrictive. Real-world causal factors often exhibit complex distributional characteristics that cannot be adequately captured by a unimodal Gaussian. To address this, we propose the Flow-based Exogenous Prior for each concept. We model exogenous variables n_k for each causal concept k using an independent Normalizing Flow, allowing the model to capture complex, non-Gaussian densities specific to each semantic factor.

We employ a set of independent Normalizing Flow (Papamakarios et al., 2021) models $\{T_{\psi,k}\}_{k=1}^K$ to define flexible densities for exogenous variables. Let $\epsilon_k \sim \mathcal{N}(\mathbf{0}, I)$ be a base distribution for the k -th concept. The flow defines a

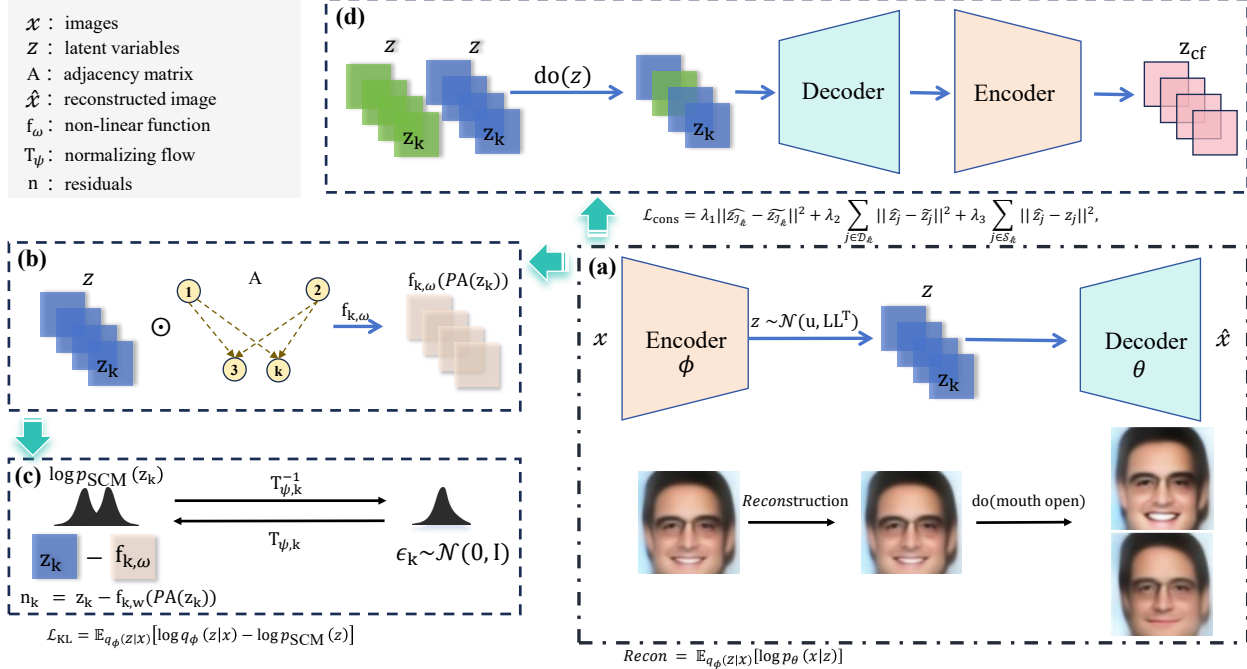


Figure 2. An overview of FlexCausal. (a) Overall Framework: The model encodes input images x into latent variables z , which are then reconstructed via the decoder. (b) Structural Causal Mechanism: The latent space is structured as a causal graph defined by the adjacency matrix A . For each node z_k , its value is determined by its parents $PA(z_k)$ through a nonlinear structural function $f_{k,ω}$. (c) Flow Prior: To model complex priors, we utilize Normalizing Flows ($T_{ψ,k}$) to transform the simple base distribution into the flexible posterior distribution of the residuals. (d) Counterfactual Consistency Constraint: This explicitly penalizes violations of structural equations under intervention, thereby ensuring the reliability of generated counterfactuals.

bijective mapping $n_k = T_{ψ,k}^{-1}(\epsilon_k)$. The log-likelihood of a noise sample n_k is given by the change of variables formula:

$$\log p_{ψ,k}(n_k) = \log p(\epsilon_k) + \log \left| \det \frac{\partial T_{ψ,k}^{-1}(\epsilon_k)}{\partial \epsilon_k} \right|. \quad (9)$$

Recall the structural equation for the k -th concept: $n_k = z_k - f_k(\{z_j \mid A_{jk} = 1\})$. Due to the independence of exogenous noise terms, the joint likelihood is $\log p_{SCM}(z) = \sum_{k=1}^K \log p_{SCM}(z_k)$. Applying the change of variables from n_k to z_k , one has:

$$\log p_{SCM}(z) = \log p_{ψ,k}(n_k) + \log \left| \det \frac{\partial n_k}{\partial z_k} \right|. \quad (10)$$

Using Proposition 3.6, the Jacobian term vanishes. This yields a computationally efficient objective for the prior:

$$\log p_{SCM}(z) = \sum_{k=1}^K \log p_{ψ,k}(z_k - f_k(z_j \mid A_{jk} = 1)). \quad (11)$$

This factorization allows us to decouple the learning of the causal mechanism from the learning of the distributional statistics. The model can then fit arbitrary complex exogenous distributions for each concept individually.

4.3. Consistency Loss

To ensure the decoder faithfully renders these causal interventions without introducing spurious correlations, we propose a Counterfactual Consistency Mechanism. This mechanism constrains the generative process by enforcing structural invariance.

Definition 4.1 (Causal Partition). Given the causal graph G , for a specific intervention on the latent variable z_k , the latent space Z is partitioned into three disjoint subsets

(1) Intervention Set (\mathcal{I}_k): The singleton set containing the target variable itself, i.e., $\mathcal{I}_k = \{z_k\}$.

(2) Descendant Set (\mathcal{D}_k): The set of variables strictly downstream from z_k , defined as $\mathcal{D}_k = \{z_j \in Z \mid z_k \rightarrow \dots \rightarrow z_j \text{ in } G\}$.

(3) Invariant Set (\mathcal{S}_k): The complement set containing variables structurally independent of the intervention, defined as $\mathcal{S}_k = Z \setminus (\mathcal{I}_k \cup \mathcal{D}_k)$.

Based on the proposed partition, we stipulate that any intervention on z_k must satisfy three key constraints. Specifically, interventional alignment for \mathcal{I}_k across the decode and re-encode cycle, structural propagation for \mathcal{D}_k governed by the

SCM, and strict invariance for the invariant set \mathcal{S}_k . Given a counterfactual latent code \tilde{z} (derived by intervening on z_k and fully propagating effects through the SCM), we decode it into an image x_{cf} and re-encode it to obtain \tilde{z} . The total consistency loss is formulated as:

$$\begin{aligned}\mathcal{L}_{\text{cons}} &= \lambda_1 \|\hat{z}_{\mathcal{I}_k} - \tilde{z}_{\mathcal{I}_k}\|^2 + \lambda_2 \sum_{j \in \mathcal{D}_k} \|\hat{z}_j - \tilde{z}_j\|^2 \\ &+ \lambda_3 \sum_{j \in \mathcal{S}_k} \|\hat{z}_j - z_j\|^2,\end{aligned}\quad (12)$$

where z_j is the j -th factor of the latent code z , \tilde{z}_j is the ideal counterfactual value dictated by the causal graph, and z_j is the original source value.

4.4. Optimization Objective

The Flow-based Prior is integrated into the Block-Diagonal VAE framework by modifying the KL divergence term in the Evidence Lower Bound (ELBO). We employ the Monte Carlo estimation for the KL divergence instead of an analytical computation, as the integration of the Flow-based prior's log-likelihood with the encoder's variational density yields no closed-form solution. Given a batch of posterior samples $z \sim q_\phi(z|x)$ from the Block-Diagonal Encoder, the prior matching loss is defined as:

$$\begin{aligned}\mathcal{L}_{\text{KL}} &= \mathbb{E}_{q_\phi(z|x)} [\log q_\phi(z|x) - \log p_{\text{SCM}}(z)] \\ &= \mathbb{E}_{q_\phi(z|x)} \left[\log q_\phi(z|x) - \sum_{k=1}^K \log p_{\psi,k}(n_k) \right].\end{aligned}\quad (13)$$

Intuitively, this objective encourages the encoder to produce latent codes z such that, after removing the causal effects of parents, the remaining residuals n follow a distribution that can be explained by the Flow model. This allows the framework to accommodate distributionally robust causal disentanglement representation learning, properly identifying factors even when they follow highly non-Gaussian statistics (e.g., Laplace or Bimodal), as validated in our experiments. To learn the model parameters, we maximize the Evidence Lower Bound (ELBO) on the marginal likelihood. Substituting our Flow-based SCM prior into the KL divergence term, we obtain the following tractable training objective:

$$\text{ELBO} = \mathbb{E}_{q_\phi(z|x)} [\log p_\theta(x|z)] - \beta \mathcal{L}_{KL}. \quad (14)$$

Since encoder $q_\phi(z|x)$ infers latent variables solely from images, we introduce a supervision loss to explicitly align the learned causal blocks z_k with the ground-truth u_k . This ensures that each subspace z_k semantically encodes the specific factor designated by u_k :

$$\mathcal{L}_{\text{sup}} = \mathbb{E}_{q_\phi(z|x)} \left[\sum_{k=1}^K \|h_k(z_k) - u_k\|^2 \right], \quad (15)$$

where $h_k(\cdot)$ is a linear auxiliary predictor that maps the vector-valued z_k to the label space of u_k .

To enforce the mutual independence derived from Assumption 3.3, we introduce the Hilbert-Schmidt Independence Criterion (HSIC) (Gretton et al., 2005) loss $\mathcal{L}_{\text{HSIC}}$. This term explicitly minimizes the statistical dependence among exogenous variables during training. Finally, the total loss function $\mathcal{L}_{\text{total}}$ is as follows:

$$\mathcal{L}_{\text{total}} = \mathcal{L}_{\text{recon}} + \beta \cdot \mathcal{L}_{\text{KL}} + \lambda \cdot \mathcal{L}_{\text{cons}} + \gamma \cdot \mathcal{L}_{\text{sup}} + \nu \cdot \mathcal{L}_{\text{HSIC}}, \quad (16)$$

where β , γ , λ , and ν are hyperparameters. The detailed derivation is provided in Appendix A.

4.5. Manifold-Aware Directional Intervention

Although the hard intervention ($do(z_k = c)$) employed in previous methods is theoretically grounded, the inherent sparsity of the learned latent space often renders such forced scalar assignments prone to projecting latent codes off the data manifold, leading to out-of-distribution decoding and unrealistic generation. To mitigate this, we propose a Manifold-Aware Directional Intervention mechanism. This mechanism treats intervention as a dynamic traversal along a semantic vector field rather than a static assignment, effectively constraining the manipulation path within high-density data regions. Specifically, we capture a global direction $v_k \in \mathbb{R}^{d_k}$ representing the natural semantic variation of each factor k (e.g., the transition from "Young" to "Old") via a momentum-based estimation strategy during training. By identifying sample subsets corresponding to the Top-K and Bottom-K ground-truth values within each batch, we continuously update their respective global expectations, μ_k^{pos} and μ_k^{neg} , via Exponential Moving Average (EMA). The vector difference between these expectations is ultimately established as the robust direction for natural semantic variation.

$$\begin{aligned}\mu_k^{\text{pos}} &\leftarrow (1 - \alpha) \mu_k^{\text{pos}} + \alpha \cdot \mathbb{E}_{z \in \mathcal{B}_{\text{top}}}[z_k], \\ \mu_k^{\text{neg}} &\leftarrow (1 - \alpha) \mu_k^{\text{neg}} + \alpha \cdot \mathbb{E}_{z \in \mathcal{B}_{\text{btm}}}[z_k],\end{aligned}\quad (17)$$

where α is a momentum coefficient. $\mathcal{B}_{\text{top}}^{(k)}$ and $\mathcal{B}_{\text{btm}}^{(k)}$ denote the subsets of latent variables corresponding to the data points with the highest and lowest values of the ground-truth label u_k , respectively. The direction of intervention is defined as $\mathbf{v}_k = \mu_k^{\text{pos}} - \mu_k^{\text{neg}}$ and the Manifold-Aware Directional Intervention is then formalized as follows:

$$do(z_k = z_k + \tau \cdot \mathbf{v}_k), \quad (18)$$

where τ is a scalar intensity. This fosters geometric alignment between the intervention path and the intrinsic data manifold.

Table 1. Quantitative Comparison on Synthetic and Real-World Datasets. Note that the results of CausalDiffAE and CIDiffuser on Pendulum dataset are quoted from (Huang et al., 2025).

Method	Filter			Pendulum		CelebA (Smile)		CelebA (Age)	
	MIC (\uparrow)	TIC (\uparrow)	WD (\downarrow)	MIC (\uparrow)	TIC (\uparrow)	MIC (\uparrow)	TIC (\uparrow)	MIC (\uparrow)	TIC (\uparrow)
CausalDiffAE	-	-	-	91.10 \pm 0.00	89.20 \pm 0.00	-	-	-	-
CIDiffuser	-	-	-	98.10 \pm 0.00	86.50 \pm 0.00	-	-	-	-
SCMVAE	89.39 \pm 1.25	63.20 \pm 0.33	89.29 \pm 0.40	81.47 \pm 0.42	76.40 \pm 1.48	52.61 \pm 0.62	43.65 \pm 0.58	38.10 \pm 0.61	29.71 \pm 0.57
CausalVAE	95.61 \pm 0.20	76.87 \pm 0.05	82.40 \pm 0.09	91.06 \pm 1.21	82.08 \pm 0.39	57.65 \pm 0.36	48.51 \pm 0.21	41.78 \pm 0.56	33.04 \pm 0.53
FlexCausal (Ours)	98.88 \pm 0.10	89.54 \pm 0.02	57.99 \pm 0.40	98.94 \pm 0.49	90.13 \pm 0.53	60.26 \pm 0.58	54.86 \pm 0.55	41.56 \pm 0.32	37.23 \pm 0.22

5. Experiment

5.1. Experimental Setup

5.1.1. DATASETS.

Filter is a synthetic benchmark created using Blender (Community, 2018) to evaluate causal representation learning under challenging distributional constraints. The dataset consists of 12,000 images at $128 \times 128 \times 4$ resolution, generated by 6 ground-truth latent causal variables. The underlying causal structure is defined as: (filter size, filter position) \rightarrow (shadow size), and (filter color, background color) \rightarrow (shadow color). Distinctively, the generative factors follow bimodal and multimodal Gaussian distributions, creating a challenging disjoint latent structure for representation learning. Detailed information is provided in the Appendix C.

Pendulum (Yang et al., 2021) is a synthetic dataset which consists of four causal factors. The underlying causal structure is defined as: (Pendulum Angle, Light Position) \rightarrow (Shadow Length, Shadow Position).

CelebA (Liu et al., 2015) is a large-scale face attributes dataset containing more than 200k celebrity images with 40 binary attribute annotations. Specifically, we construct two distinct subsets, CelebA-Smile and CelebA-Age, to instantiate different causal mechanisms. CelebA-Smile focuses on facial expression dependencies. The underlying causal graph is defined as: (Smile, Gender) \rightarrow (Narrow Eyes), (Smile) \rightarrow (Mouth Open), and (Mouth Open) \rightarrow (Narrow Eyes). CelebA-Age models demographic causal effects. The causal structure is defined as: (Age, Gender) \rightarrow (Bald, Beard). For implementation, we randomly select 30,000 images from the dataset to constitute our training and testing sets.

5.1.2. METRICS.

We employ three complementary metrics to quantitatively assess the quality of learned causal representations. To evaluate identifiability and capture complex dependencies, we utilize the Mean Correlation Coefficient (MIC) and Total Information Coefficient (TIC) (Kinney & Atwal, 2014). Both measure the degree of information correlation between la-

tent variables and ground truth. To validate the effectiveness of our Flow-based prior, we compute the Wasserstein Distance (WD) (Arjovsky et al., 2017) between latent variables and ground-truth distributions.

5.1.3. IMPLEMENTATION DETAILS.

We implemented FlexCausal using the PyTorch (Paszke et al., 2019) framework on a single NVIDIA RTX 4090 GPU. For the backbone architecture, we employed a CNN as the encoder. To facilitate structural disentanglement, we utilized an independent additive decoder. The exogenous prior is parameterized by a stack of 4 Masked Autoregressive Flow (MAF) blocks (Papamakarios et al., 2017) to enable flexible density estimation. We took AdamW (Loshchilov & Hutter, 2017) as the optimizer with an initial learning rate of 1×10^{-3} . To ensure stable convergence, we adopted a cosine annealing scheduler paired with a linear warmup strategy. Details of network architectures and hyperparameter settings are provided in Appendix C

5.2. Experimental Results

We compare our model with SCM-VAE and CausalVAE across all datasets (Filter, CelebA-Smile, CelebA-Age, and Pendulum). Additionally, on the Pendulum dataset, we extend the comparison to include recent diffusion-based approaches, CIDiffuser and CausalDiffAE, to further evaluate our performance against generative diffusion baselines.

Quantitative results demonstrate that FlexCausal achieves the best performance on MIC, TIC, and WD metrics across all benchmarks. On Filter and CelebA datasets, FlexCausal outperforms SCM-VAE and CausalVAE, particularly in terms of MIC and TIC, validating its robust causal disentanglement and identifiability. Notably, on the Filter dataset, FlexCausal surpasses other methods in terms of WD. This confirms that our Flow-based Prior effectively captures complex ground-truth distributions comparable to other frameworks while maintaining the explicit structural control of SCMs.

Table 2. Ablation Study on Filter Dataset.

Metrics	MIC (\uparrow)	TIC (\uparrow)	WD (\downarrow)
FlexCausal (Ours)	98.88 \pm 0.10	89.54 \pm 0.02	57.99 \pm 0.40
w/o Flow Prior	91.88 \pm 2.07	75.81 \pm 2.36	60.29 \pm 1.96
w/o Consistency Loss	97.41 \pm 0.32	88.31 \pm 1.31	58.31 \pm 0.28
w/o Block-Diagonal	98.19 \pm 0.19	89.05 \pm 0.03	58.50 \pm 0.47

5.3. Ablation Study

As shown in Table 2, to evaluate the efficacy of each core component, we conducted an ablation study on the Filter dataset. Removing the Flow-based Prior yields the most significant performance degradation, marked by a drop in the TIC score and a significant deterioration in WD. This empirically confirms that standard Gaussian priors fail to capture complex exogenous noise, underscoring the indispensability of the flow model for precise structural identification and distribution matching. Furthermore, the exclusion of the Counterfactual Consistency Loss leads to declines in both MIC and TIC, validating the critical role of explicit structural penalties in ensuring robust causal disentanglement. Although removing the block diagonal mechanism yields only minor effects, the complete model demonstrates superior performance across all metrics, providing compelling evidence that the synergistic interaction of these components is indispensable for achieving robust causal generation.

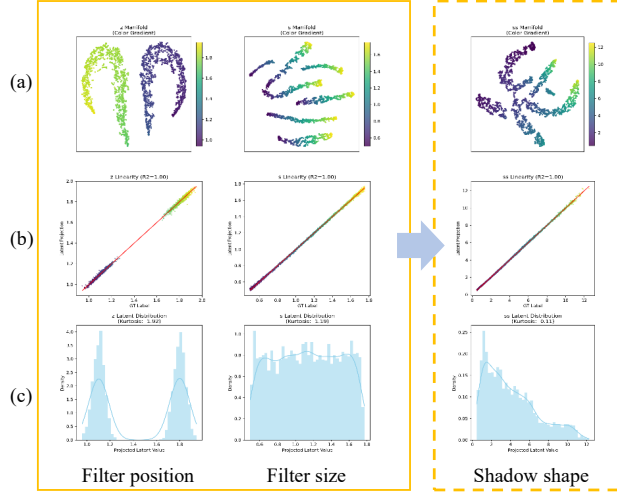


Figure 3. Visualization of the Learned Latent Space on the Filter Dataset. (a) Latent Manifold Topology: The t-SNE visualization reveals the manifold structure of latent space. (b) GT-Latent Alignment: The scatter plots demonstrate a strong linear correlation between latent projections and ground truth labels (with $R^2 > 0.99$ for almost every concept), confirming precise semantic alignment. (c) Posterior Density: The learned latent distribution closely matches the ground truth distribution of the underlying factors, verifying the expressive capability of our Flow-based prior to model complex non-Gaussian densities.

5.4. Visualization on Complex Distributions

To verify FlexCausal’s capability in modeling non-Gaussian and complex distributions, we visualize the learned latent space on the Filter dataset. As illustrated in Figure 3, we project the high-dimensional latent variables into 2D/1D spaces to analyze their geometric and statistical properties from three distinct perspectives. We first employ t-SNE (Maaten & Hinton, 2008) to visualize the global manifold structure of each latent block. As observed in Figure 3(a), FlexCausal effectively captures the intrinsic topology of the data, forming a smooth and continuous manifold. Second, to assess disentanglement, we perform a linear regression between latent variables and GT. Figure 3(b) exhibits a strong linear correlation, with determination coefficients reaching near perfection ($R^2 > 0.99$) in almost all concepts. This indicates that FlexCausal achieves a near-isometric mapping, effectively disentangling semantic factors into orthogonal directions. Third, the posterior density in Figure 3(c) demonstrates that the learned latent distribution highly aligns with the true underlying distribution of the GT factors (e.g. bimodal). This validates that our Flow-based prior successfully captures the authentic statistical properties of the data, avoiding both posterior collapse and the bias typically introduced by standard Gaussian regularization.

6. Conclusions

In this paper, we proposed FlexCausal, a novel CDRL framework designed to overcome the limitations of rigid Gaussian assumptions in Causal Disentangled Representation Learning. By synergizing a Block-Diagonal VAE with the flexible Flow-based Exogenous Prior, our approach effectively models complex non-Gaussian distributions while preserving the semantic integrity of vector-valued concepts. Furthermore, we introduced a Manifold-Aware Directional Intervention strategy to ensure structurally consistent and physically plausible counterfactual generation. Extensive experiments on our proposed Filter benchmark and standard real-world datasets demonstrate that FlexCausal outperforms other CRDL methods.

References

Arjovsky, M., Chintala, S., and Bottou, L. Wasserstein generative adversarial networks. In *International Conference on Machine Learning*, pp. 214–223. PMLR, 2017.

Bengio, Y., Courville, A., and Vincent, P. Representation learning: A review and new perspectives. *IEEE Transactions on Pattern Analysis and Machine Intelligence*, 35 (8):1798–1828, 2013.

Bhowal, P., Soni, A., and Rambhatla, S. Why do variational

autoencoders really promote disentanglement? In *Proceedings of the 41st International Conference on Machine Learning*, volume 235, pp. 3817–3849, 2024.

Buchholz, S., Rajendran, G., Rosenfeld, E., Aragam, B., Schölkopf, B., and Ravikumar, P. Learning linear causal representations from interventions under general nonlinear mixing. *Advances in Neural Information Processing Systems*, 36:45419–45462, 2023.

Community, B. O. *Blender - a 3D modelling and rendering package*. Blender Foundation, Stichting Blender Foundation, Amsterdam, 2018. URL <http://www.blender.org>.

De Sousa Ribeiro, F., Xia, T., Monteiro, M., Pawlowski, N., and Glocker, B. High fidelity image counterfactuals with probabilistic causal models. In *Proceedings of the 40th International Conference on Machine Learning*, volume 202 of *Proceedings of Machine Learning Research*, pp. 7390–7425, 23–29 Jul 2023. URL <https://proceedings.mlr.press/v202/de-sousa-ribeiro23a.html>.

Duan, Y., Wang, L., Zhang, Q., and Li, J. Factorvae: A probabilistic dynamic factor model based on variational autoencoder for predicting cross-sectional stock returns. In *Proceedings of the AAAI Conference on Artificial Intelligence*, volume 36, pp. 4468–4476, 2022.

Fan, D., Kou, Y., and Gao, C. Causal flow-based variational auto-encoder for disentangled causal representation learning. *ACM Transactions on Intelligent Systems and Technology*, 16(5):1–26, 2025.

Goodfellow, I., Pouget-Abadie, J., Mirza, M., Xu, B., Warde-Farley, D., Ozair, S., Courville, A., and Bengio, Y. Generative adversarial networks. *Communications of the ACM*, 63(11):139–144, 2020.

Gretton, A., Bousquet, O., Smola, A., and Schölkopf, B. Measuring statistical dependence with hilbert-schmidt norms. In *International Conference on Algorithmic Learning Theory*, pp. 63–77. Springer, 2005.

Higgins, I., Matthey, L., Pal, A., Burgess, C., Glorot, X., Botvinick, M., Mohamed, S., and Lerchner, A. betavae: Learning basic visual concepts with a constrained variational framework. In *International Conference on Learning Representations*, 2017.

Ho, J., Jain, A., and Abbeel, P. Denoising diffusion probabilistic models. *Advances in Neural Information Processing Systems*, 33:6840–6851, 2020.

Hoyer, P., Janzing, D., Mooij, J. M., Peters, J., and Schölkopf, B. Nonlinear causal discovery with additive noise models. *Advances in Neural Information Processing Systems*, 21, 2008.

Huang, S., Li, H., Zheng, C., Wang, L., Liao, G., Gong, Z., Yang, H., and Liu, L. Visual representation learning through causal intervention for controllable image editing. In *Proceedings of the Computer Vision and Pattern Recognition Conference*, pp. 23484–23493, 2025.

Kinney, J. B. and Atwal, G. S. Equitability, mutual information, and the maximal information coefficient. *Proceedings of the National Academy of Sciences*, 111(9):3354–3359, 2014.

Kocaoglu, M., Snyder, C., Dimakis, A. G., and Vishwanath, S. CausalGAN: Learning causal implicit generative models with adversarial training. In *International Conference on Learning Representations*, 2018. URL <https://openreview.net/forum?id=BJE-4xW0W>.

Komanduri, A., Wu, Y., Huang, W., Chen, F., and Wu, X. Scm-vae: Learning identifiable causal representations via structural knowledge. In *2022 IEEE International Conference on Big Data (Big Data)*, 2022.

Komanduri, A., Wu, Y., Chen, F., and Wu, X. Learning causally disentangled representations via the principle of independent causal mechanisms. In *Proceedings of the 33rd International Joint Conference on Artificial Intelligence*, 2024a.

Komanduri, A., Zhao, C., Chen, F., and Wu, X. Causal diffusion autoencoders: Toward counterfactual generation via diffusion probabilistic models. *ArXiv*, abs/2404.17735, 2024b. URL <https://api.semanticscholar.org/CorpusID:269449555>.

Kori, A., Balsells-Rodas, C., Glocker, B., Li, Y., and Locatello, F. Causal representation learning and inference via mixture-based priors. In *ICLR 2025 Workshop on Deep Generative Model in Machine Learning: Theory, Principle and Efficacy*, 2025. URL <https://openreview.net/forum?id=jtXQiPwTRM>.

Li, X., Sun, S., and Feng, R. Causal representation learning via counterfactual intervention. In *Proceedings of the AAAI Conference on Artificial Intelligence*, volume 38, pp. 3234–3242, 2024.

Lippe, P., Magliacane, S., Löwe, S., Asano, Y. M., Cohen, T., and Gavves, E. Causal representation learning for instantaneous and temporal effects in interactive systems. In *The Eleventh International Conference on Learning Representations*, 2023. URL <https://openreview.net/forum?id=itZ6ggvMnzS>.

Liu, X., Yuan, J., An, B., Xu, Y., Yang, Y., and Huang, F. C-disentanglement: Discovering causally-independent generative factors under an inductive bias of confounder. *Advances in Neural Information Processing Systems*, 36:39566–39581, 2023.

Liu, Z., Luo, P., Wang, X., and Tang, X. Deep learning face attributes in the wild. In *Proceedings of the IEEE International Conference on Computer Vision*, pp. 3730–3738, 2015.

Locatello, F., Bauer, S., Lucic, M., Raetsch, G., Gelly, S., Schölkopf, B., and Bachem, O. Challenging common assumptions in the unsupervised learning of disentangled representations. In *International Conference on Machine Learning*, pp. 4114–4124. PMLR, 2019.

Loshchilov, I. and Hutter, F. Decoupled weight decay regularization. *arXiv preprint arXiv:1711.05101*, 2017.

Maaten, L. v. d. and Hinton, G. Visualizing data using t-sne. *Journal of Machine Learning Research*, 9(Nov): 2579–2605, 2008.

Pan, Y. and Bareinboim, E. Counterfactual image editing. *arXiv preprint arXiv:2403.09683*, 2024.

Pan, Y. and Bareinboim, E. Counterfactual image editing with disentangled causal latent space. In *The Thirty-ninth Annual Conference on Neural Information Processing Systems*, 2025. URL <https://openreview.net/forum?id=u2Lgi4NIe7>.

Papamakarios, G., Pavlakou, T., and Murray, I. Masked autoregressive flow for density estimation. *Advances in Neural Information Processing Systems*, 30, 2017.

Papamakarios, G., Nalisnick, E., Rezende, D. J., Mohamed, S., and Lakshminarayanan, B. Normalizing flows for probabilistic modeling and inference. *Journal of Machine Learning Research*, 22(57):1–64, 2021.

Paszke, A., Gross, S., Massa, F., Lerer, A., Bradbury, J., Chanan, G., Killeen, T., Lin, Z., Gimelshein, N., Antiga, L., et al. Pytorch: An imperative style, high-performance deep learning library. *Advances in Neural Information Processing Systems*, 32, 2019.

Pearl, J. *Causality*. Cambridge university press, 2009.

Schölkopf, B., Locatello, F., Bauer, S., Ke, N. R., Kalchbrenner, N., Goyal, A., and Bengio, Y. Toward causal representation learning. *Proceedings of the IEEE*, 109(5): 612–634, 2021.

Shen, X., Liu, F., Dong, H., Lian, Q., Chen, Z., and Zhang, T. Weakly supervised disentangled generative causal representation learning. *Journal of Machine Learning Research*, 23(241):1–55, 2022.

Shen, Y., Gu, J., Tang, X., and Zhou, B. Interpreting the latent space of gans for semantic face editing. In *2020 IEEE/CVF Conference on Computer Vision and Pattern Recognition (CVPR)*, pp. 9240–9249, 2020. doi: 10.1109/CVPR42600.2020.00926.

Song, Y., Sohl-Dickstein, J., Kingma, D. P., Kumar, A., Ermon, S., and Poole, B. Score-based generative modeling through stochastic differential equations. In *International Conference on Learning Representations*, 2021. URL <https://openreview.net/forum?id=PxTIG12RRHS>.

Yang, M., Liu, F., Chen, Z., Shen, X., Hao, J., and Wang, J. Causalvae: Disentangled representation learning via neural structural causal models. In *2021 IEEE/CVF Conference on Computer Vision and Pattern Recognition (CVPR)*, pp. 9588–9597, 2021. doi: 10.1109/CVPR46437.2021.00947.

Zhang, K., Xie, S., Ng, I., and Zheng, Y. Causal representation learning from multiple distributions: A general setting. In *Forty-first International Conference on Machine Learning*, 2024. URL <https://openreview.net/forum?id=Pte6iiXvpf>.

A. Derivation of Total Objective

A.1. Derivation of the ELBO Objective

Our goal is to maximize the marginal log-likelihood of the observed data x , denoted as $\log p_\theta(x)$. Since the true posterior $p_\theta(z|x)$ is intractable, we introduce a variational distribution $q_\phi(z|x)$ to approximate it. Starting from the log-likelihood:

$$\begin{aligned}\log p_\theta(x) &= \log \int p_\theta(x, z) dz \\ &= \log \int q_\phi(z|x) \frac{p_\theta(x, z)}{q_\phi(z|x)} dz \\ &= \log \mathbb{E}_{z \sim q_\phi(z|x)} \left[\frac{p_\theta(x, z)}{q_\phi(z|x)} \right].\end{aligned}\tag{19}$$

Applying Jensen's Inequality, we obtain the Evidence Lower Bound (ELBO):

$$\begin{aligned}\log p_\theta(x) &\geq \mathbb{E}_{z \sim q_\phi(z|x)} \left[\log \frac{p_\theta(x, z)}{q_\phi(z|x)} \right] \\ &= \mathbb{E}_{z \sim q_\phi(z|x)} [\log p_\theta(x|z) + \log p_{\text{SCM}}(z) - \log q_\phi(z|x)] \\ &= \underbrace{\mathbb{E}_{q_\phi(z|x)} [\log p_\theta(x|z)]}_{\text{Reconstruction Term}} - \underbrace{D_{\text{KL}}(q_\phi(z|x) \| p_{\text{SCM}}(z))}_{\text{Regularization Term}},\end{aligned}\tag{20}$$

where the reconstruction term is computed using the Mean Squared Error(MSE). The core challenge lies in computing the KL divergence term, given that our prior $p_{\text{SCM}}(z)$ is a complex implicit distribution defined by a Normalizing Flow, and our posterior $q_\phi(z|x)$ has a structured block-diagonal form. The KL divergence term can be expanded as follows:

$$D_{\text{KL}}(q_\phi(z|x) \| p_{\text{SCM}}(z)) = \mathbb{E}_{z \sim q_\phi} [\log q_\phi(z|x) - \log p_{\text{SCM}}(z)].\tag{21}$$

Below, we derive the computation for terms $\log q_\phi(z|x)$ and $\log p_{\text{SCM}}$ respectively.

A.2. Computation of Variational Log-Density $\log q_\phi(z|x)$

We assume the variational posterior factorizes over K causal concept blocks, $q_\phi(z|x) = \prod_{k=1}^K \mathcal{N}(z_k; \mu_k, \Sigma_k)$, where each covariance matrix is parameterized by a lower triangular Cholesky factor L_k such that $\Sigma_k = L_k L_k^\top$.

We reparameterize z_k for each block using a standard Gaussian noise vector $\epsilon_k \sim \mathcal{N}(0, I)$:

$$z_k = \mu_k + L_k \epsilon_k.\tag{22}$$

The log-density of the Gaussian sample z_k is given by:

$$\log q_\phi(z_k|x) = -\frac{d_k}{2} \log(2\pi) - \frac{1}{2} \log |\Sigma_k| - \frac{1}{2} (z_k - \mu_k)^\top \Sigma_k^{-1} (z_k - \mu_k).\tag{23}$$

By substituting the reparameterization equation ($z_k - \mu_k = L_k \epsilon_k$) and the covariance factorization ($\Sigma_k = L_k L_k^\top$), the quadratic term simplifies as follows:

$$\begin{aligned}(z_k - \mu_k)^\top \Sigma_k^{-1} (z_k - \mu_k) &= (L_k \epsilon_k)^\top (L_k L_k^\top)^{-1} (L_k \epsilon_k) \\ &= \epsilon_k^\top L_k^\top (L_k^\top)^{-1} L_k^{-1} L_k \epsilon_k \\ &= \epsilon_k^\top \epsilon_k = \|\epsilon_k\|^2.\end{aligned}\tag{24}$$

Recall that the log-determinant of the covariance matrix simplifies via the Cholesky factor:

$$\log |\Sigma_k| = \log |L_k L_k^\top| = 2 \sum_{i=1}^{d_k} \log(L_k)_{ii}.\tag{25}$$

Substituting the simplified quadratic term ($\|\epsilon_k\|^2$) and the log-determinant term back into the definition of the multivariate Gaussian log-density, we obtain the closed-form expression for block k :

$$\begin{aligned}\log q_\phi(z_k|x) &= -\frac{d_k}{2} \log(2\pi) - \frac{1}{2} \log |\Sigma_k| - \frac{1}{2} (z_k - \mu_k)^\top \Sigma_k^{-1} (z_k - \mu_k) \\ &= -\frac{d_k}{2} \log(2\pi) - \sum_{i=1}^{d_k} \log(L_k)_{ii} - \frac{1}{2} \|\epsilon_k\|^2.\end{aligned}\quad (26)$$

Finally, summing over all K causal concept blocks, the total variational log-density is:

$$\log q_\phi(z|x) = \sum_{k=1}^K \left(-\frac{d_k}{2} \log(2\pi) - \sum_{i=1}^{d_k} \log(L_k)_{ii} - \frac{1}{2} \|\epsilon_k\|^2 \right). \quad (27)$$

This final form is computationally efficient as it relies solely on the predicted diagonal elements of L_k and the sampled noise vectors ϵ_k .

A.3. Computation of $\log p_{\text{SCM}}(z)$

Recall Equation 11, the SCM prior likelihood $\log p_{\text{SCM}}(z)$ is formulated as:

$$\log p_{\text{SCM}}(z) = \sum_{k=1}^K \log p_{\psi,k}(z_k - f_k(z_j \mid A_{jk} = 1)). \quad (28)$$

A.4. KL divergence term Estimation

Combining the derived entropy term above and the SCM prior likelihood, the KL divergence is estimated via Monte Carlo sampling over a batch of size B :

$$D_{\text{KL}}(q_\phi(z|x) \mid\mid p_{\text{SCM}}(z)) \approx \frac{1}{B} \sum_{b=1}^B \left(\log q_\phi(z^{(b)} \mid x^{(b)}) - \log p_{\text{SCM}}(z^{(b)}) \right), \quad (29)$$

where $z^{(b)}$ represents the reparameterized samples. This estimation enables efficient end-to-end optimization of both the encoder and the SCM parameters.

A.5. Final Training Objective

Integrating ELBO with the proposed causal constraints, the final differentiable loss function is defined as:

$$\mathcal{L}_{\text{total}} = \underbrace{\|x - D_\theta(z)\|^2}_{\text{Reconstruction}} + \underbrace{\beta (\log q_\phi(z|x) - \log p_{\text{SCM}}(z))}_{\text{KL Divergence}} + \lambda \mathcal{L}_{\text{cons}} + \gamma \mathcal{L}_{\text{sup}} + \nu \mathcal{L}_{\text{HSIC}}, \quad (30)$$

where constants are omitted for brevity, and z is the reparameterized sample $z = \mu + L\epsilon$. Hyperparameters $\beta, \lambda, \gamma, \nu$ control the trade-off between reconstruction quality, distribution matching, and structural constraints.

B. Proof of Proposition

B.1. Proof of Proposition 3.6

Proof. Let $z = [z_1^\top, \dots, z_K^\top]^\top$ be the latent vector partitioned into K causal blocks, where $z_k \in \mathbb{R}^{d_k}$ and the total dimension is $D = \sum_{k=1}^K d_k$. Let $\mathbf{J} \in \mathbb{R}^{D \times D}$ denote the Jacobian matrix of the transformation mapping the latent variables z to the exogenous noise n , defined block-wise as $\mathbf{J}_{ij} = \frac{\partial n_i}{\partial z_j}$. Recall Equation 2:

$$n_k = z_k - f_k(\text{PA}(z_k)). \quad (31)$$

The diagonal block \mathbf{J}_{kk} represents the partial derivative of n_k with respect to z_k . Differentiating the structural equation yields:

$$\mathbf{J}_{kk} = \frac{\partial n_k}{\partial z_k} = \frac{\partial (z_k - f_k(\text{PA}(z_k)))}{\partial z_k} = \mathbf{I}_{d_k} - \frac{\partial f_k(\text{PA}(z_k))}{\partial z_k}, \quad (32)$$

where \mathbf{I}_{d_k} is the $d_k \times d_k$ identity matrix. Due to the acyclicity of the causal graph \mathcal{G} , a variable z_k cannot be its own parent (i.e., $z_k \notin \text{PA}(z_k)$). $f_k(\text{PA}(z_k))$ is independent of z_k , implying $\frac{\partial f_k}{\partial z_k} = \mathbf{0}$. Thus, the diagonal blocks simplify to:

$$\mathbf{J}_{kk} = \mathbf{I}_{d_k}. \quad (33)$$

Assume the indices $1, \dots, K$ follow a valid topological ordering of the graph \mathcal{G} . For any $j > i$, the variable z_j implies a node downstream or unrelated to z_i , and thus cannot be a parent of z_i . Therefore, n_i is independent of z_j , which implies:

$$\mathbf{J}_{ij} = \frac{\partial n_i}{\partial z_j} = \mathbf{0} \quad \text{for all } j > i. \quad (34)$$

Finally, we obtain:

$$\det(\mathbf{J}) = \prod_{k=1}^K \det(\mathbf{J}_{kk}) = \prod_{k=1}^K \det(\mathbf{I}_{d_k}) = \prod_{k=1}^K 1 = 1. \quad (35)$$

Since the Jacobian determinant is unity, we conclude that the transformation is volume-preserving. \square

C. Detailed Information

C.1. Filter Dataset

To evaluate the model's capability in handling complex physical interactions and non-standard latent distributions, we introduce the **Filter** dataset. As shown in Figure 4, this dataset is synthetically generated using the Blender 3D creation suite with the Cycles physics-based rendering engine. The dataset contains 12,000 high-quality rendered images with a resolution of $128 \times 128 \times 4$ (RGBA). The inclusion of the alpha channel and the high-fidelity ray-traced shadows provides rich supervision for learning fine-grained causal mechanisms.

Data Generation Process. The scene consists of a translucent equilateral triangular filter, a fixed point light source, and a receiving surface. The dataset focuses on capturing the causal interplay between the geometry of the occluder and the resulting projection. The underlying Structural Causal Model (SCM) involves 4 independent exogenous variables (parents) and 2 dependent endogenous variables (children):

- **Filter Size (S):** The side length of the equilateral triangle, sampled from a continuous uniform distribution.
- **Filter Position (H):** The vertical distance of the filter from the base, sampled from a bimodal distribution.
- **Filter Color (C_f):** The RGB absorption properties of the filter.
- **Background Color (C_b):** The albedo color of the ground surface.
- **Shadow Shape (A_s):** Determined by the interaction between S and H under the perspective projection of the point light ($A_s := f(S, H)$).
- **Shadow Color (C_s):** Resulting from the subtractive color mixing of the light passing through the filter onto the colored base ($C_s := g(C_f, C_b)$).

Distributional Challenges. Unlike standard datasets that often assume unimodal Gaussian latents, CausalFilter is specifically designed to challenge representation learning algorithms by enforcing bimodal and multimodal Gaussian distributions on key causal variables. Specifically, the Filter Position is sampled from two distinct modes ($z \in \{1.1, 1.8\}$ with Gaussian noise), and Filter Color is sampled from three distinct clusters (Red, Blue, and Yellow). This creates a discontinuous and disjoint manifold structure in the ground-truth latent space, rigorously testing the model's ability to learn disentangled representations and perform valid counterfactual generation across diverse modes.

C.2. Implement Detail

Table 3 details the specific architecture of the Encoder and Decoder used in our experiments. For the Flow-based prior, we utilized a Masked Autoregressive Flow (MAF) with 4 layers.

We list the hyperparameters used for training in Table 4.

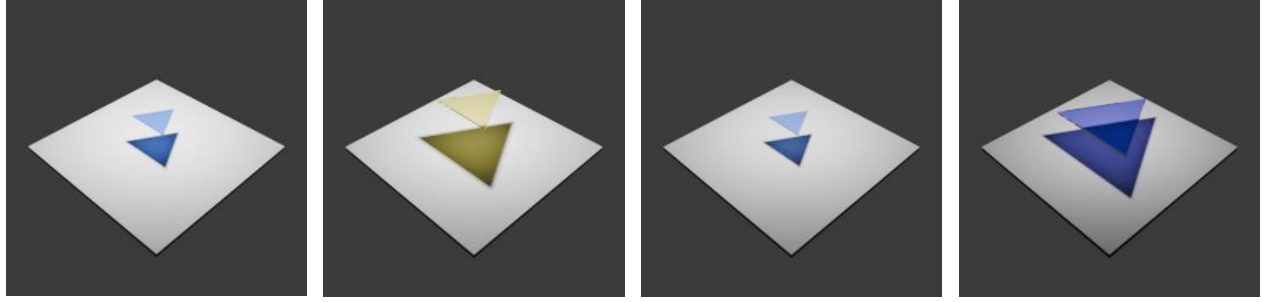


Figure 4. Filter Dataset

Table 3. Network Architecture of FlexCausal (CelebA 128x128). The model consists of a shared encoder backbone and an independent additive decoder. Causal concepts and other concepts share the backbone but use distinct prediction heads. K denotes the number of causal concepts. For simplicity, we employ a standard VAE to encode other concepts in CelebA that are not part of the SCM.

Stage	Layer	Output Shape
Encoder		
Shared Backbone	Input Image	$3 \times 128 \times 128$
	Conv2d(3, 32, k=3, s=2), BN, LeakyReLU	$32 \times 64 \times 64$
	ResBlock(32, 64, s=2)	$64 \times 32 \times 32$
	ResBlock(64, 128, s=2)	$128 \times 16 \times 16$
	ResBlock(128, 256, s=2)	$256 \times 8 \times 8$
Prediction Heads	Conv2d(256, 512, k=3, s=2), BN, LeakyReLU	$512 \times 4 \times 4$
	Flatten \rightarrow Linear \rightarrow Split(μ, σ)	$K \times z_{dim}, K \times z_{dim} \times z_{dim}$
Decoder		
Independent Projectors	Linear($z_{dim}, 8192$) \rightarrow Reshape	$K \times (512 \times 4 \times 4)$
	Additive Fusion: $\sum_{k=1}^K \text{Feat}_k$	$512 \times 4 \times 4$
Upsampling Body	Upsample(2x), Conv(512, 256), ResBlock	$256 \times 8 \times 8$
	Upsample(2x), Conv(256, 128), ResBlock	$128 \times 16 \times 16$
	Upsample(2x), Conv(128, 64), ResBlock	$64 \times 32 \times 32$
	Upsample(2x), Conv(64, 32), ResBlock	$32 \times 64 \times 64$
	Upsample(2x), Conv(32, 3), Tanh	$3 \times 128 \times 128$

Table 4. Hyperparameter Settings. The Hyperparameter configuration(CelebA).

Hyperparameter	Value
Batch Size	64
Total Epochs	100
Normalizing Flow Layers	4
Latent Dimension	16
Consistency Loss Weight (λ_1)	1.0
Consistency Loss Weight (λ_2)	10.0
Consistency Loss Weight (λ_3)	1.0
KL Loss Weight (β)	0.1
Sup Loss Weight (γ)	3000

D. Additional Experimental Results

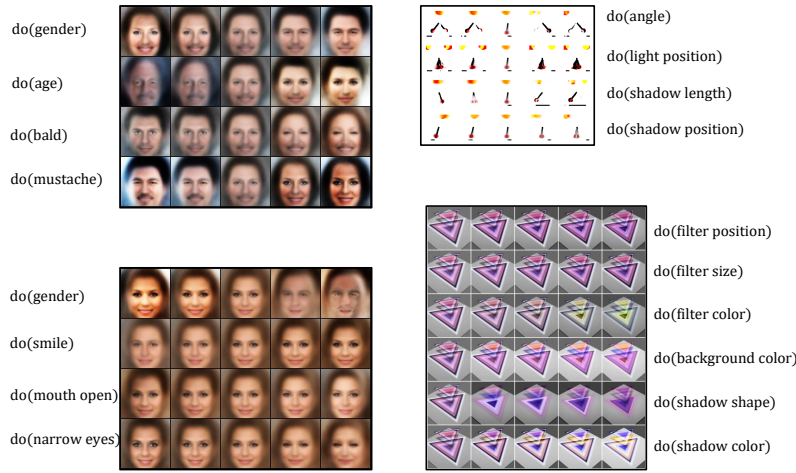


Figure 5. Results of CausalVAE on CelebA-Smile, CelebA-Age, Pendulum, Filter

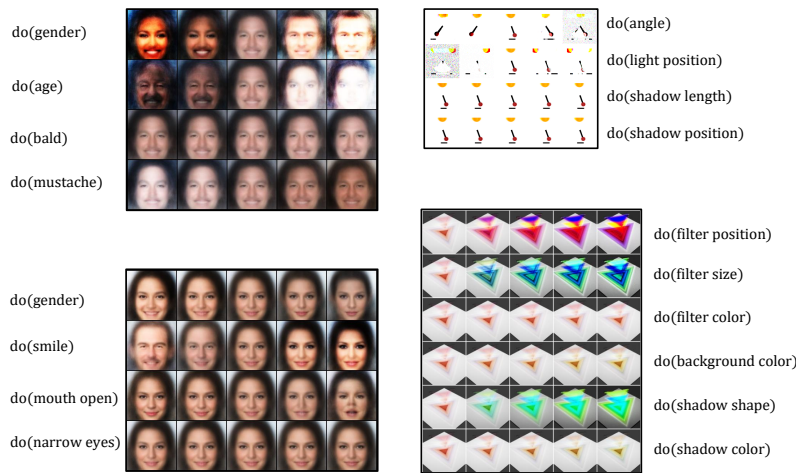
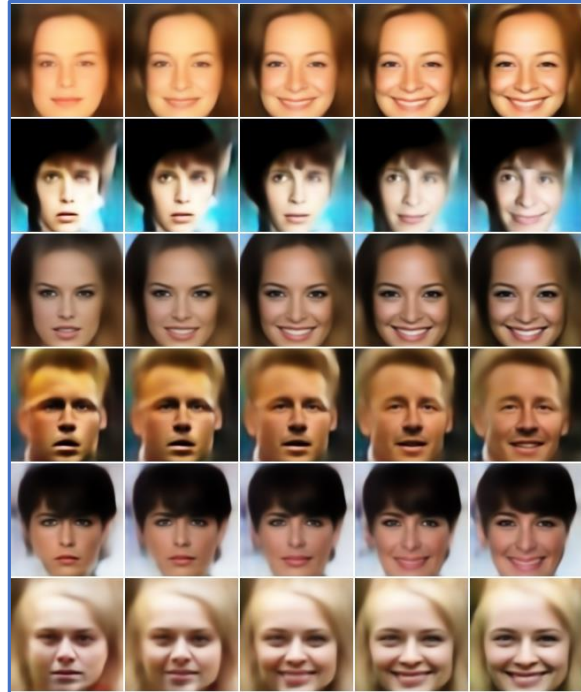


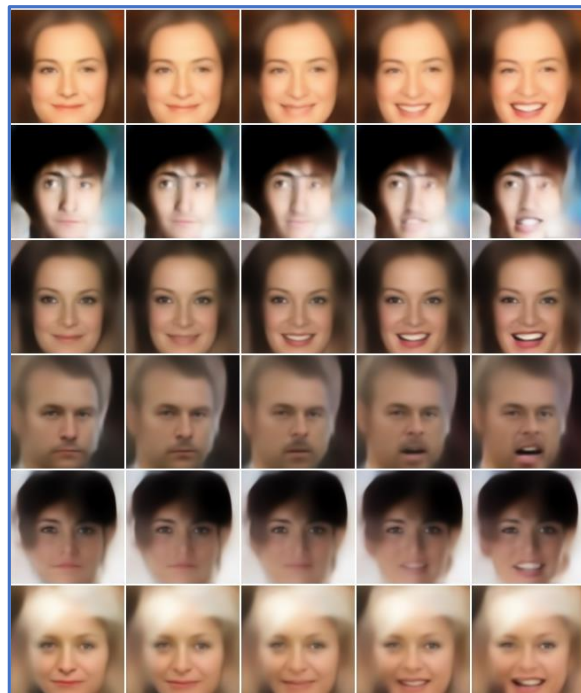
Figure 6. Results of SCVAE on CelebA-Smile, CelebA-Age, Pendulum, Filter



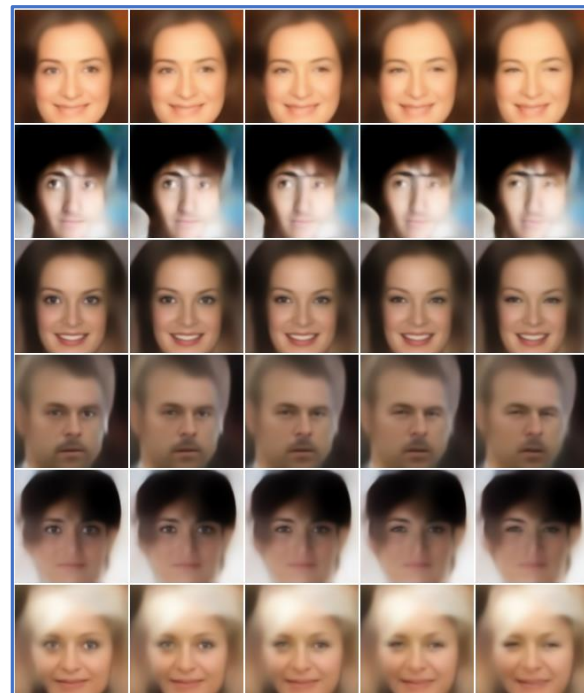
do(smile)



do(gender)



do(mouth open)



do(narrow eyes)

Figure 7. Results of our FlexCausal on CelebA-Smile

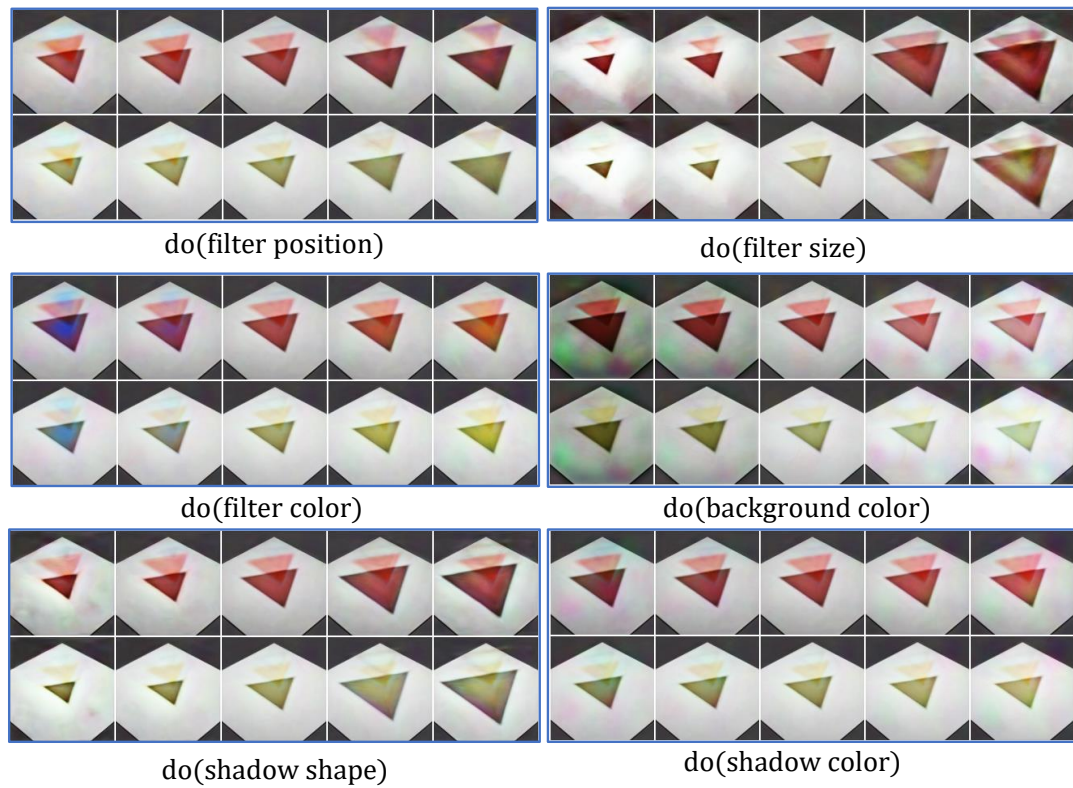


Figure 8. Results of our FlexCausal on Filter

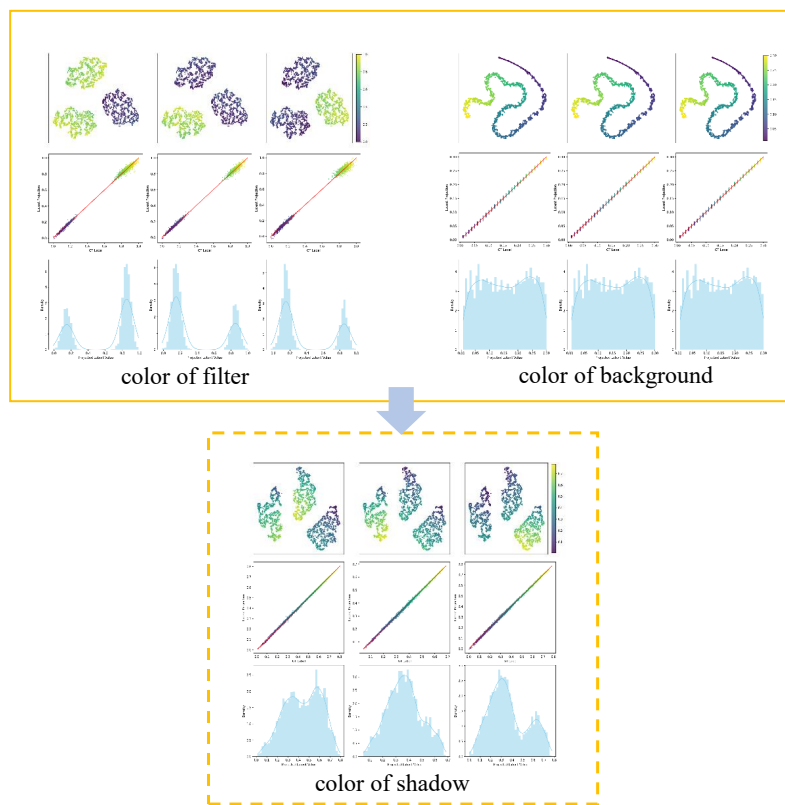


Figure 9. Visualization of Filter color, Background color, Shadow color

E. Algorithm

E.1. FlexCausal Pretrain Algorithm

Algorithm 1 Training Procedure for FlexCausal

Require: Dataset $\mathcal{D} = \{x^{(i)}, u^{(i)}\}_{i=1}^N$, Adjacency Matrix A , Momentum α , Hyperparams $\beta, \lambda, \gamma, \nu$.

```

1: Initialize: Encoder  $\phi$ , Decoder  $\theta$ , SCM parameters  $\omega$ , Flow parameters  $\psi$ .
2: Initialize: Global manifold centroids  $\mu_k^{\text{pos}}, \mu_k^{\text{neg}} \leftarrow \mathbf{0}$  for  $k = 1, \dots, K$ .
3: for epoch= 1 to  $M$  do
4:   Sample mini-batch  $\{x, u\} \sim \mathcal{D}$ .
5:   // Block-Diagonal Encoding
6:    $\mu_\phi, \Sigma_\phi \leftarrow \text{Encoder}_\phi(x)$ 
7:   Sample latent variables:  $z_k \leftarrow \mu_k + L_k \cdot \epsilon_k, \quad \epsilon_k \sim \mathcal{N}(0, I)$ .
8:   // Manifold-Aware Direction Update
9:   for  $k = 1$  to  $K$  do
10:    Identify Top/Bottom-K indices:
11:     $\mathcal{I}_{\text{top}} \leftarrow \text{Top-K Indices}(u_k); \quad \mathcal{I}_{\text{btm}} \leftarrow \text{Bottom-K Indices}(u_k)$ .
12:    Compute batch expectations:
13:     $\mathbb{E}_{\text{top}} \leftarrow \text{Mean}(z_k[\mathcal{I}_{\text{top}}]); \quad \mathbb{E}_{\text{btm}} \leftarrow \text{Mean}(z_k[\mathcal{I}_{\text{btm}}])$ .
14:    Update global directions:
15:     $\mu_k^{\text{pos}} \leftarrow \alpha \mu_k^{\text{pos}} + (1 - \alpha) \mathbb{E}_{\text{top}}; \mu_k^{\text{neg}} \leftarrow \alpha \mu_k^{\text{neg}} + (1 - \alpha) \mathbb{E}_{\text{btm}}$ 
16:    Update inference vector:  $\mathbf{v}_k \leftarrow \mu_k^{\text{pos}} - \mu_k^{\text{neg}}$ 
17:   end for
18:   // Flow-based Prior Evaluation
19:   for  $k = 1$  to  $K$  do
20:     Get parents:  $\text{PA}(z_k) \leftarrow \{z_j \mid A_{jk} = 1\}$ .
21:     Compute residual:  $n_k \leftarrow z_k - f_{\omega, k}(\text{PA}(z_k))$ .
22:     Evaluate Flow likelihood:  $\ell_k \leftarrow \log p(T_\psi(n_k)) + \log |\det J_{T_\psi}|$ .
23:      $\log p_{\text{SCM}}(z) \leftarrow \log p_{\text{SCM}}(z) + \ell_k$ 
24:   end for
25:   // Counterfactual Consistency
26:   Construct  $z_{\text{cf}}^{(k)}$ : Set  $z_{\text{cf}}^{(k)} \leftarrow \tilde{z}^{(k)}$ , keep invariants  $z_{\text{cf}}^{(\neg \text{desc})} \leftarrow z^{(\neg \text{desc})}$ , and update children  $z_{\text{cf}}^{(\text{desc})}$ .
27:   Re-encode:  $\hat{z}_{\text{cf}} \leftarrow E_\phi(D_\theta(z_{\text{cf}}))$ .
28:   // Loss Computation
29:    $\mathcal{L}_{\text{KL}} \leftarrow \mathbb{E}_{q_\phi}[\log q_\phi(z|x) - \log p_{\text{SCM}}(z)]$ 
30:    $\mathcal{L}_{\text{recon}} \leftarrow -\log p_\theta(x|z)$ .
31:    $\mathcal{L}_{\text{cons}} \leftarrow \|\hat{z}_{\text{cf}}^{(k)} - \tilde{z}^{(k)}\|^2 + \|\hat{z}_{\text{cf}}^{(\neg \text{desc})} - z^{(\neg \text{desc})}\|^2 + \|\hat{z}_{\text{cf}}^{(\text{desc})} - z_{\text{cf}}^{(\text{desc})}\|^2$ .
32:    $\mathcal{L}_{\text{sup}} \leftarrow \sum_{k=1}^K \|h_k(z_k) - u_k\|^2$ .
33:   // Optimization
34:    $\mathcal{L}_{\text{total}} \leftarrow \mathcal{L}_{\text{recon}} + \beta \mathcal{L}_{\text{KL}} + \lambda \mathcal{L}_{\text{sup}} + \gamma \mathcal{L}_{\text{cons}} + \nu \mathcal{L}_{\text{HSIC}}$ .
35:   Update parameters  $\phi, \theta, \omega, \psi \leftarrow \text{Optimizer}(\nabla \mathcal{L}_{\text{total}})$ .
36: end for

```
